Surfaces and Interfaces 51 (2024) 104791

Contents lists available at ScienceDirect

Surfaces and Interfaces

journal homepage: www.sciencedirect.com/journal/surfaces-and-interfaces

Determining the atomic coordination number in the structure of β_{12} borophene on Ag(111) via X-ray photoelectron diffraction analysis

Luca Bignardi [a,b], Monica Pozzo [c,d,e], Albert Zelenika [a,1], Francesco Presel [a,2], Paolo Lacovig [b], Silvano Lizzit [b], Dario Alfè [c,f], Alessandro Baraldi [a,b,*]

[a] Department of Physics, University of Trieste, via Valerio 2, 34127, Trieste, Italy
[b] Elettra Sincrotrone Trieste, AREA Science Park, 34149, Basovizza, Trieste, Italy
[c] Department of Earth Sciences, University College London, 5 Gower Place, WC1E 6BS, London, United Kingdom
[d] Faculty of Technological & Innovation Sciences, Universitas Mercatorum, Piazza Mattei 10, 00186 Rome, Italy
[e] Institute for Materials Discovery, UCL East, Marshgate Building, 7 Siding Street, Stratford, London, E20 2AE, United Kingdom
[f] Dipartimento di Fisica "Ettore Pancini", Università Federico II, Via Cinthia 21, 80126, Napoli, Italy

ARTICLE INFO

Keywords:
Borophene
2D materials
Photoelectron spectroscopy
XPS
Photoelectron diffraction
DFT

ABSTRACT

This study investigates the electronic properties of the borophene β_{12} phase on Ag(111) and correlates them with specific structural features by combining high-resolution core-level photoelectron spectroscopy, X-ray photoelectron diffraction, and density functional theory-based calculations. We establish a link between the atomic coordination number of the non-equivalent B atoms in the β_{12} unit cell and the observed spectroscopic signatures in the B 1s spectrum. This finding is conclusively proven by photoelectron diffraction, which confirms that this polymorph exhibits minimal corrugation on Ag(111). These results contribute to a deeper understanding of the properties of various borophene structures on metallic substrates and may stimulate further studies in realizing nanoscaled structures where the atomic coordination number plays a central role.

1. Introduction

Borophene stands out as one of the most intriguing members among two-dimensional (2D) materials, collecting significant attention due to its potential applications across various fields such as nanoelectronics, energy storage, and catalysis [1–7]. In contrast to graphene, a semimetal, and to hexagonal boron nitride (hBN), a large-gap insulator, borophene is predicted to exhibit metallic properties, making it often considered the lightest 2D metal ever produced [8–10]. Boron's adaptability in forming diverse chemical bonds in bulk is well-established, with several 3D boron allotropes predicted and investigated [11]. Thus, a wide array of planar 2D boron polymorphs, each featuring unique atomic arrangements, was largely predicted by theoretical investigations. Such variety of polymorphs shows a broad number of local geometries and the B atoms can form bonds with nearest neighbors with an atomic coordination number (CN) of 3, 4, 5 and 6 [12]. This morphological plurality in borophene leads to intriguing electronic properties like Dirac fermions [13–15] and superconductivity [16,17]. Its exceptional mechanical properties [18,19], coupled with excellent conductivity, position borophene as a prime candidate for flexible electronic devices.

The first direct synthesis of borophene on a surface occurred on Ag(111) using molecular beam epitaxy (MBE) [20–22], a method which has proven very effective in achieving high quality films with extended in-phase domains in other 2D materials. This first realization and later investigations revealed that the choice of substrate temperature growth in ultra-high vacuum (UHV) are a critical parameter in determining the structural properties of the borophene layer grown. The aforementioned experiments of deposition on Ag(111) showed the dominant formation of two different crystalline phases depending on the substrate temperature during the MBE growth.

Each borophene polymorph's specific structure seems to activate distinct electronic properties. Penev et al. [9] conducted comprehensive first-principles calculations, identifying three stable polymorphs: α-borophene, β_{12}-borophene, and χ_3-borophene. These polymorphs exhibit diverse lattice structures and bonding characteristics, leading to distinctive electronic properties. α-borophene showcases hexagonal rings of boron atoms with alternating in-plane and out-of-plane buckling, inducing anisotropic bonding—a blend of strong covalent interactions within the plane and weaker interplanar interactions, displaying metallic behavior. On the contrary, β_{12} borophene adopts a

* Corresponding author at: Department of Physics, University of Trieste, via Valerio 2, 34127, Trieste, Italy.
E-mail address: alessandro.baraldi@elettra.eu (A. Baraldi).
[1] Current address: Department of Physics, Technical University of Denmark, Fysikvej, building 311 2800 Kgs. Lyngby, Denmark.
[2] Current address: Institute of Physics, Graz University, Univ.-Platz 5, 8010 Graz, Austria.

https://doi.org/10.1016/j.surfin.2024.104791
Received 25 April 2024; Received in revised form 28 June 2024; Accepted 12 July 2024
Available online 18 July 2024

triangular lattice with hexagonal vacancies, displaying semiconducting properties. The vacancies expose boron atoms, enhancing the sheet's chemical reactivity and potential catalytic applications [21]. Lastly, the χ_3 polymorph features a rhombohedral lattice structure, exhibiting metallic behavior [9]. Such vacancies in the layer leads to chain-like structures in β_{12} and χ_3 borophene, resulting in strongly anisotropic structure [23].

Despite numerous theoretical predictions for freestanding 2D borophene, this material lacks thermodynamic stability, unlike boron bulk compounds and, consequently, borophene cannot be mechanically exfoliated like graphene and cannot exist as unsupported material [24]. Furthermore, the peculiar nature of the B-B bonds leads to buckling of boron atoms, which is also influenced by the chosen substrate [25]. This emphasizes the pivotal role played by the substrate in determining the grown layer's morphological phase and, consequently, its specific electronic properties. The investigation of properties of the interfaces formed by borophene and its supporting material, from both morphological and electronic perspectives, is thus recognized as a crucial step in the characterization of the properties of this material and linking all these aspects becomes extremely important.

In the last years, it has been shown that the β_{12} structure is among the energetically favorable structures that borophene can form on Ag(111), with a small structural buckling and a high density of hexagonal vacancies [25–27]. Small corrugation is a distinctive features of β_{12} borophene on Ag(111), which can form much more corrugated polymorphs on other metals [22]. Strong buckling and therefore a strong periodic corrugation in the layer might alter the electronic properties of borophene because of the consequent strain induced in the B-B bonds. Similarly, in graphene, corrugation can lead to significant effects such as the opening of a band gap, electron–hole puddles and carriers scattering [28]; therefore, a comprehensive investigation on the structure on the correlation between the structure of borophene polymorphs on substrates and their electronic properties is still of central relevance.

In this paper we investigate the features of β_{12} borophene epitaxially grown on Ag(111), employing synchrotron-based high-resolution X-ray photoelectron spectroscopy (HR-XPS), low-energy electron diffraction (LEED), and X-ray photoelectron diffraction (XPD) measurements with a two-fold purpose. Our first goal is to experimentally establish a correlation between the observed electronic structure in XPS and the coordination number of this borophene phase. Moreover, we aim to investigate the possibility to individuate the spectroscopic features induced by buckling. To complement these experimental efforts, we incorporate density functional theory (DFT) calculations, shedding further light on this specific interface.

2. Methods

2.1. Experimental methods

The experiments were carried out in the UHV experimental chamber of the SuperESCA beamline at the Elettra synchrotron-radiation facility in Trieste, Italy, maintaining a base pressure of approximately 1×10^{-10} mbar during the experiments. The Ag(111) single crystal underwent cleaning cycles involving Ar^+ ion sputtering (E_B = 1 keV) and subsequent thermal annealing (870 K, for 10 min.) to ensure surface purity, confirmed via XPS. Borophene epitaxial growth occurred by evaporating B atoms from a boron rod (American Elements, purity 2N8) onto the Ag surface in UHV conditions using an electron-bombardment evaporator. XPS, LEED, and XPD measurements were conducted within the same UHV chamber where the samples were grown. The B 1s spectra were acquired using various photon energies, as detailed later in the manuscript. The sample was mounted on a five degrees of freedom manipulator, enabling acquisition of core-level spectra with diverse azimuthal (ϕ) and polar (θ) emission angles of photoelectrons for generating XPD patterns. The overall energy resolution at the beamline was ca. 50 meV. Core-level photoemission spectra were collected using a Phoibos hemispherical electron energy analyzer from SPECS (150 mm mean radius), equipped with an in-house developed delay-line detector, enabling high-resolution fast data acquisition during processes such as gas exposure and temperature ramps of the sample [29].

The core-level photoemission spectra were fitted employing a linear combination of Gaussian-convoluted Doniach–Sunjic (DS) profiles [30]. These profiles consist of a Lorentzian curve accounting for finite core-hole lifetime effects, an asymmetry parameter describing low-energy electron–hole pair excitations near the Fermi level, and a Gaussian distribution representing phonon, instrumental, and inhomogeneous broadening. Inelastic contributions were modeled using a Shirley background [31].

XPD patterns were obtained through 50 azimuthal scans across a range of polar emission angles, from grazing emission (θ = 70°) to normal emission (θ = 0°), encompassing a wide azimuthal sector (ϕ = 100°) measuring the B 1s core level region for about 1000 different angles. Peak fit analysis was performed for each spectrum, extracting the angle-dependent intensity $I(\theta,\phi)$ of each component from the fit, i.e. the area under each photoemission spectral component, in an interval between +2 and −3 eV with respect to the maximum of the spectral peak. The intensity was used to derive the modulation function $\chi = \frac{I(\theta,\phi)-I_0(\theta)}{I_0(\theta)}$ for each emission angle, where $I_0(\theta)$ is the average intensity for each azimuthal scan. The determination of the crystalline structure involved the comparison between measured XPD patterns with multiple scattering simulations using the Electron Diffraction in Atomic Clusters (EDAC) package [32]. The geometry of the cluster used for simulations is reported in Supplementary Material. The agreement between simulations and experimental results was quantified using the reliability factor (R), which is defined as $R = \frac{\sum_i \left(\chi_{exp,i}-\chi_{sim,i}\right)^2}{\sum_i \left(\chi^2_{exp,i}+\chi^2_{sim,i}\right)}$, where $\chi_{exp,i}$ and $\chi_{sim,i}$ are the experimental and the calculated modulation functions for each data point i, respectively [33]. The variance of the minimum R-factor (ΔR_{min}) stemming from the analysis was calculated [34], as detailed in the Supplementary Material. Low-energy electron diffraction (LEED) experiments were conducted using a commercial VG instrument installed within the SuperESCA beamline experimental chamber.

2.2. Theoretical methods

Density functional theory calculations were performed with the VASP code [35]. To describe the surface, we used the usual slab geometry, with a topmost layer including 75 B atoms, over a 4-layer Ag slab. The two bottom layers of Ag were kept frozen at their bulk geometry, with a lattice parameter of 2.948 Å, and the rest of the system was fully relaxed using the PBE until the largest residual force was less than 0.015 eV/Å. We employed the projector augmented method (PAW) [36] using PBE [37] potentials. The plane wave cutoff was set to 319 eV, and the relaxations were performed by sampling the Brillouin zone using a 3 × 3 × 1 grid. Core-electron BEs have been estimated in the final-state approximation, therefore including also final state effects due to core–hole screening.

3. Results and discussion

β_{12} borophene was obtained by directly depositing atomic B produced by an MBE evaporator on the Ag(111) substrate kept at 600 K, while monitoring the growth via fast-XPS acquisition of the B 1s core level (Fig. 1a). The temperature of the substrate has been chosen to achieve the β_{12} phase, as already described by several works [20,21,27,38]. The photon energy used to acquire HR-XPS spectra was $h\nu$ = 250 eV and the data were collected at normal electron emission, i.e. with the sample surface coinciding with the axis of the analyzer lenses. The B 1s spectra reported in Fig. 1a were acquired every five minutes since the beginning of B evaporation and each spectrum

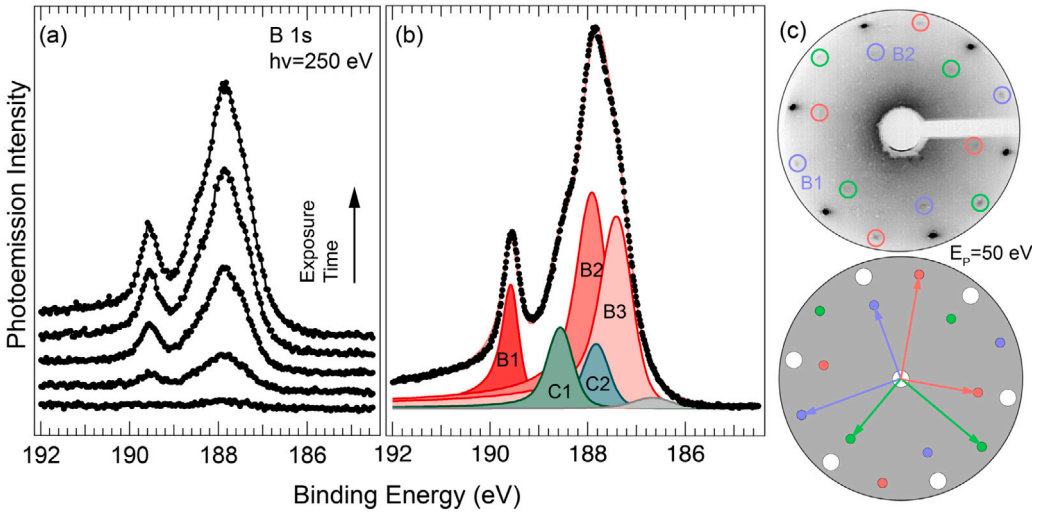

Fig. 1. (a) B 1s core level acquired via fast-XPS during the exposure of Ag(111) to B atoms, with the substrate at 600 K. Each spectrum is shifted in the vertical direction with respect to the previous one for clarity. (b) High-resolution B 1s core level spectrum acquired after the growth. The various components B1, B2, B3 belong to the β_{12} phase of borophene, while C1 and C2 are assigned to the presence of adventitious χ_3 borophene. (c) LEED pattern acquired on the borophene layer prepared at 600 K. The different colored spots are associated to the three different equivalent crystalline domains of β_{12} borophene. The energy of the electron primary beam was 50 eV.

reported was acquired in ca. 15 s, with the total deposition amounting up to about 30 min, for a calculated final coverage of 0.7 ML, corresponding to a growth rate of 0.02 ML/min. By comparing this spectrum to that one obtained by borophene exposed to atmospheric conditions [21,39], we can conclude that no signal associated with the formation of boron oxides (BE=192.3 eV) was detected. The B-related signal is observed since the early stages of the evaporation process. This can be seen as an indication that B does not diffuse into the bulk. Markedly, no significant differences in the lineshape of the B 1s were observed during the entire process, which is the fingerprint that the borophene β_{12} phase grew by islands formation, thanks to the high mobility of B feedstock on the substrate surface at 600 K. Such type of growth is considerably different from the outcomes observed on another noble metal such as Au(111). In that case, with the substrate kept at the same temperature we used, B atoms dissolve in the Au bulk and the borophene layer is formed by B segregation only once the substrate cools down. The growth, in that case, results in borophene islands that are incorporated in the first atomic Au layer [40].

The spectral analysis of the high-resolution B 1s core level (Fig. 1b) for this layer shows three main components at a binding energy (BE) of 189.55 eV (B1), 187.95 eV (B2), and 187.52 eV (B3). Moreover, we also observed two smaller components C1 and C2, with a BE=188.46 and 187.66 eV, respectively. The binding energy of the B1, B2 and B3 components is compatible with the formation of β_{12} phase [38], which appears to be predominant on the surface. On the other hand, the C1 and C2 features can be associated to the presence of an adventitious χ_3 phase, and that can obtained by exposing the Ag(111) surface kept at 740 K to B (see Electronic Supplementary Material for the B 1s spectrum acquired in that case). The formation of the β_{12} phase was confirmed by acquiring LEED patterns (top panel in Fig. 1c), in line with the outlines of earlier reports in the same system [20,21,38]. Besides the main Ag(111) spots, three sets of borophene-related diffraction beams appeared after the growth. Each set of spots, marked with red, blue, and green circles, was associated with the rectangular unit cell of the β_{12} phase. A simulated LEED pattern using as input such a phase is shown at the bottom of the figure and matches the experimental outcomes, returning a Park matrix equal to $M = \begin{pmatrix} 0.63 & 1.38 \\ 0.89 & 0 \end{pmatrix}$. Markedly, although observed in XPS, no sign of χ_3 phase was detected in LEED patterns: this might be indicative of the formation of extremely small crystalline domains for the χ_3 phase.

More information on the electronic properties and morphology of the β_{12} borophene phase were obtained from DFT calculations. In Fig. 2a, we report the histogram of the B-Ag vertical distance, defined as the distance from the first surface Ag layer, obtained from the calculations. We observed that most of the atoms in the unit cell are found at ca. 2.35 Å from the topmost Ag layer, with a maximum span of ca. 0.18 Å around this value. Moreover, the borophene layer does not induce any reconstruction of the Ag surface but rather leaves the positions of the Ag atoms almost unaltered. These outcomes are in line with earlier theoretical predictions [25–27] and are indicating that borophene on Ag(111) has a very small corrugation, unlike what happens on other metallic substrates; it is worth mentioning the case of borophene on Ir(111), which shows a corrugation of 1.18 Å and a distance from the topmost Ir layer of 2.1 Å [41]. By comparison, graphene on Ir(111), which is regarded as an example of minimally-corrugated graphene, has a vertical span of the C atoms of ca. 0.27 Å [42].

From DFT calculations we also extracted the average bond length of each B atom with its nearest neighbors. The map of distribution of the B-B distances in the unit cell, defined as the average distance to each neighbor, is reported in Fig. 2b. We observed a consistent variability in these distances, which appear to be strongly depending on the coordination number (CN) of each B atom, that can be deduced by inspecting the ball model of the β_{12} structure. Atoms with CN=4 show the largest B-B distances (1.75 Å), while atoms with CN=5 are characterized by shorter B-B bonds (1.66 Å). DFT calculations were also used to obtain information on the link between the B 1s core level shift of the various spectral component observed for B 1s and the coordination number of the B atoms for this borophene phase. In the crystalline structure of the β_{12} borophene we can identify three distinct groups of atoms with CN= 4, 5 and 6, respectively. Hence, it is reasonable to suppose that a distinctive core level shift is associated to each of these groups, because of the strong effects due to the CN on the electronic environment around each atom.

DFT-simulated core-level shifts for the B 1s are reported in Fig. 3a together with the measured B 1s spectrum for comparison. We observed that three very distinct set of core-level shifts were obtained, mirroring the presence of three group of non-equivalent B atoms in the β_{12} phase. By comparing the spectral analysis of the experimental data reported in Fig. 1c with the calculated shifts, we conclude that the B1, B2 and B3 components stem from B atoms with CN=6, 5 and 4, respectively. Campbell and co-authors have reached a similar conclusion for the β_{12} phase on Ag(111) [38], although, in that case, they motivated their interpretation in view of a theoretical prediction obtained for

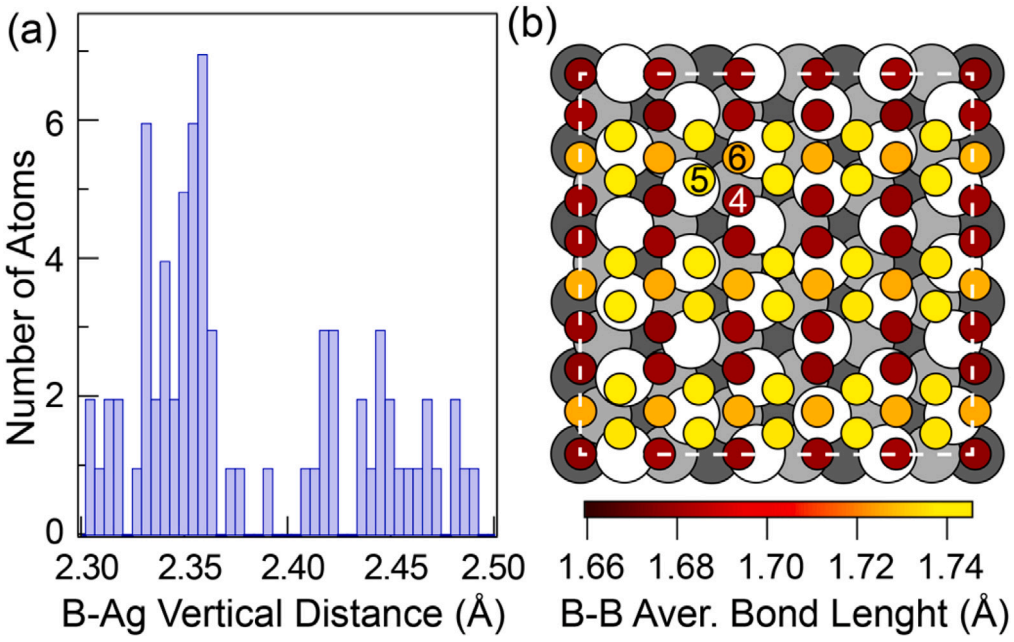

Fig. 2. (a) Histogram of the DFT-calculated distribution of the vertical distances between B atoms in the unit cell and the first Ag layer for β_{12} borophene. (b) Map of the average B-B bond length for the atoms in the β_{12} phase. The coordination number CN of the three nonequivalent B atoms in the unit cell is shown.

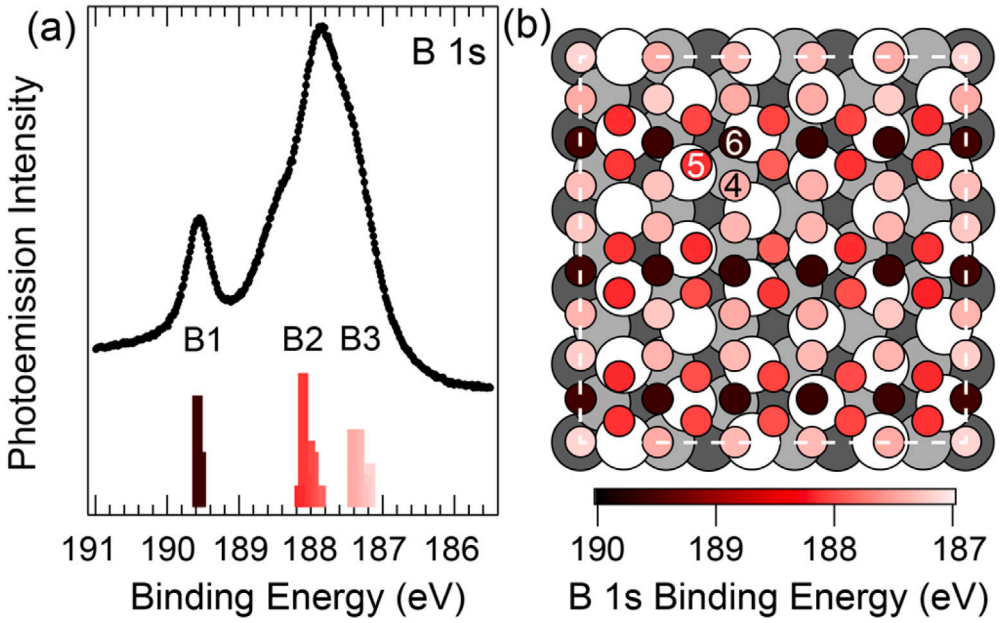

Fig. 3. (a) Calculated core level shift for B 1s superimposed to the B 1s spectrum measured after the growth. Dark red, red, and pink identifies core-level shifts associated with atoms with CN=6, 5, and 4, respectively. (b) DFT calculated B 1s binding energy for the atoms in the unit cell of β_{12} borophene. (For interpretation of the references to color in this figure legend, the reader is referred to the web version of this article.)

functionalized and defective graphene [43]. Herein, we have shown that such trend can be also applied to the case of borophene. In Fig. 3b, we show the distribution of the 1s core electron binding energy for each B atom in the borophene layer. Markedly, the differences in BE are largely determined by the CN of each atom in the layer, while the effect of the adsorption site of the B atom on the value of the BE for each atom on the Ag(111) surface is negligible, although small differences can be observed. An overall evaluation of the output of our DFT calculations seems to indicate the formation of the strong planar B-B bonds atoms and a weak interaction of this borophene phase with the Ag(111) substrate. Interestingly, the map of the B-B distances does not correlate with the map for core electron binding energies.

Experimental verification of the outcomes of the DFT calculations, also in relation to the link between the spectroscopic features observed in XPS and the structural features of the borophene layer, was obtained by means of XPD experiments. Such technique is based on the acquisition of the angle-dependent photoemission intensity modulations, which arise from the interference between the component of the photoelectron wave field that reaches the detector directly from the emitting atom and the components scattered by atoms surrounding the emitter [33,44]. This makes XPD very sensitive to the local environment surrounding the emitting atom, and thus makes it suitable to investigate the local morphology and structure of crystalline layers, even for small crystalline domains.

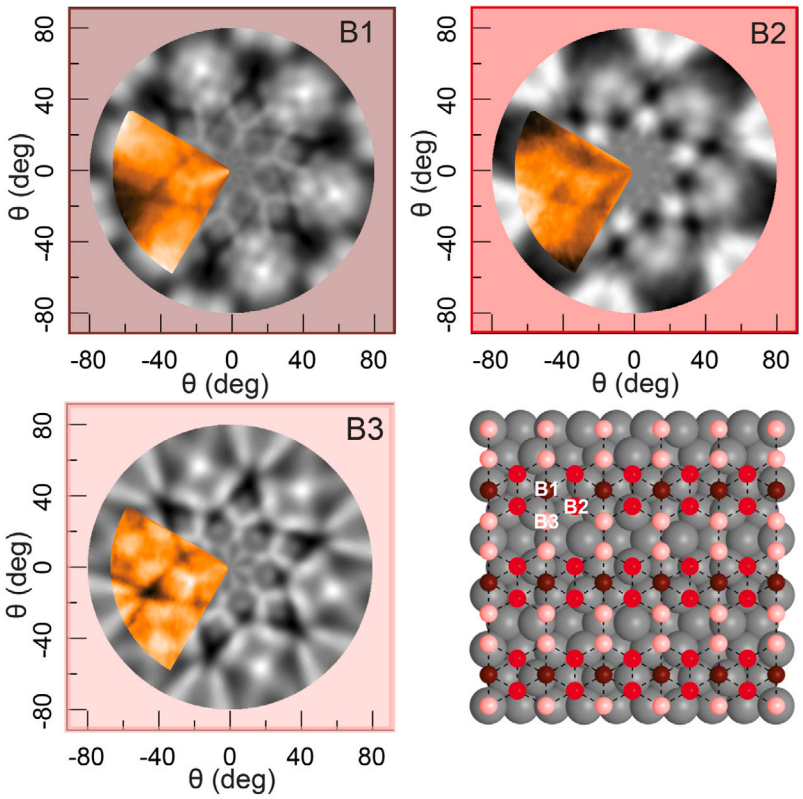

Fig. 4. Stereographic projections of the modulation function χ stemming from the B1, B2 and B3 components of the B 1s core level spectrum. The colored sector represents the experimental data, and they are superimposed to the simulated scattering patterns (grayscale) that best fit the experimental outcome. (For interpretation of the references to color in this figure legend, the reader is referred to the web version of this article.)

In Fig. 4 we report the XPD patterns obtained for the β_{12} structure, using a photon energy of 325 eV, such that the B 1s emitted electrons have a kinetic energy of ca. 135 eV, in a regime for which the electron backward scattering is enhanced [33,44]. This is the most appropriate condition to study the morphology of a 2D layer on a surface [45]. The colored sectors are experimental outcomes measured from the angular modulations of the B1, B2, and B3 components of the B 1s level reported in Fig. 1b. In order to extract information from these data, we compared the experimental results with simulated XPD patterns (grayscale sectors in Fig. 4) generated by each of the three non-equivalent atoms in the β_{12} on Ag(111) unit cell. A quantitative agreement between the simulated pattern and the experimental outcomes was obtained by means of R-factor analysis (see Methods section for details), similarly to what has been already successfully done for other 2D materials [45–51]. The initial input structure for the diffraction pattern simulations was the structure we obtained from DFT calculations. In addition to that, the simulations takes into account the three equivalent crystalline domains in borophene due to the three-fold symmetry of the Ag(111), as already observed in the LEED pattern reported in Fig. 1.

The purpose of this analysis in the context of our characterization was twofold: First, to provide a further confirmation to the results obtained via DFT linking each core level shift observed in B 1s with the CN of the B atoms. XPD is sensitive to this information, since we can simulate diffraction patterns using as emitter each different non-equivalent B atom in the unit cell of borophene, each of which has a different CN and a well-established B 1s core level shift. Secondly, we wanted to evaluate the extent of the corrugation in the borophene layer. To do so, we proceeded as follows. DFT calculations returned a distribution of B-Ag vertical distances, from which we deduced that most of the B atoms sit at 2.35 Å from the substrate. The maximum vertical buckling amplitude in that case was 0.18 Å. Therefore, we simulated XPD patterns for a series of structures in which the buckling

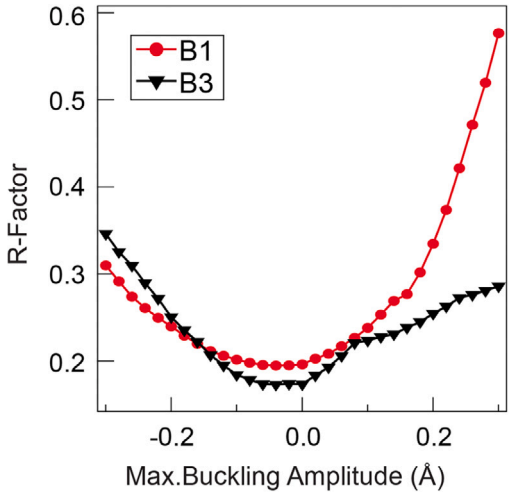

Fig. 5. R-Factor analysis of the dependence on the maximum buckling amplitude for the XPD patterns from B emitters with CN=6 (B1) and CN=4 (B3).

amplitude was varied in steps of 0.02 Å. This amplitude was zero when the structure was perfectly flat, with all the B atoms sitting at 2.35 Å from the substrate. The maximum buckling amplitude is then the difference between the vertical position of the B atom in the unit cell which is located closer to Ag and the position of the B atom that is more distant from the Ag surface plane. The XPD experiments and R-factor analysis confirmed that the core level shifts B1, B2 and B3 are to be assigned to B atoms with CN=6, 5 and 4, respectively. Moreover, we observed that the minimum R-factor, reported in Fig. 5, was obtained for the patterns B1 and B3 with a flat layer, for which the value of the

buckling is close to zero, with R = 0.195 ±0.014 and 0.179 ±0.013 for B1 and B3, respectively. This outcome is in line with the results of earlier experiments [38] that confirm the absence of corrugation for borophene on Ag(111). On the other hand, the agreement for the B2 pattern is slightly worse (R = 0.361±0.075), but we could still associate this pattern to B atoms with CN=5. We speculate that this outcome could be due to the presence of the C1 and C2 components (belonging to adventitious χ_3 borophene) overlapping with the B2 peak and whose modulations may therefore affect the diffraction-related modulations of B2. Although the indication of no corrugation stemming both from DFT and experiments is quite clear, we observe that the minimum of the R-factor curve, for both B1 and B3, is rather broad; this indicates that minimal buckling of the B atoms can take place, but it is certainly very small when compared to the buckling of borophene on other metallic surfaces [22].

These results may be instrumental to clarify several issues related to the features of the β_{12} phase on Ag(111). Such structure is reputed one of the most interesting borophene polymorphs, since it is very reactive with respect to other members of this family. Therefore, the study of reactivity of this phase to various gases are reputed of primary importance towards a full control of the properties of this material and its functionalization. Examples of these possibilities are formation of borophane, a semi-conducting layer resulting from the hydrogenation of borophene on Ag(111) [39,52], the realization of a quasi-free standing borophene bilayers on Ag(111) [53] or the studies about the reactivity of borophene to oxygen [54,55], for which one could control the anisotropic electronic transport properties by tuning the coverage of O defects [56]. The limited corrugation of β_{12} borophene on Ag(111) that we observe is a sign that the interaction with the weakly-interacting Ag substrate acts as a stabilizer of the planar B-B bonds and promotes the formation of a planar structure with strong adhesive energy to the metallic substrate [25,26]. Moreover, it has been shown that this borophene polymorph on Ag(111) seems to be more active in the hydrogen evolution reaction (HER) than the free-standing monolayer [57]. Interestingly, on the more corrugate β_{12} borophene on Cu(111), the activity towards the HER is reduced with respect to the freestanding layer [58], thus indicating that both corrugation and substrate are important factors in determining the reactivity properties of the β_{12} borophene.

4. Conclusion

In this paper, we have investigated the structure and the electronic properties of the β_{12} phase of borophene grown epitaxially on Ag(111). We showed through fast-XPS that the growth is by islands formation. The analysis of the high- resolution B 1s spectra acquired on the freshly-prepared sample was complemented by DFT calculated core level shifts, which allowed to assign a specific coordination number of the B atoms to the components observed in the B 1s spectrum. Hence, we reveal that the main item in determining the BE of the atoms in the β_{12} phase is the local atomic coordination number, while the effects of the adsorption site appear to be less important. Similarly, DFT shows that the average B-B bond length depends strongly on the CN of the atoms involved, while the calculations evidence that this borophene phase has a very limited corrugation on Ag(111). Such outcome is also confirmed by XPD experiment, which provide an experimental verification to the assumption that links the higher binding energy of the core level shift with the higher coordination number of the B atom from which the electrons are photoemitted. Interestingly, the B 1s spectra do not change their global lineshape during the entire growth process, an indication that in this phase on Ag(111) since the beginning of the growth process there are atoms with CN=4, 5 and 6. Consequently, the density and type of vacancies in the layer remains constant thoroughly. This is in agreement with what has been reported by Xu and co-authors, which have shown that the minimum-energy configurations assumed by the borophene layer on Ag(111) always include B vacancies [27]. Moreover, the same authors highlighted how calculations show that this borophene phase on Ag(111) needs to have a very small corrugation to be energetically stable, a feature that we were able to confirm experimentally by means of XPS and XPD experiments.

CRediT authorship contribution statement

Luca Bignardi: Writing – review & editing, Writing – original draft, Visualization, Investigation, Formal analysis. **Monica Pozzo:** Writing – review & editing, Formal analysis. **Albert Zelenika:** Investigation, Formal analysis. **Francesco Presel:** Writing – review & editing, Investigation. **Paolo Lacovig:** Writing – review & editing, Investigation. **Silvano Lizzit:** Writing – review & editing, Methodology, Investigation. **Dario Alfè:** Writing – review & editing, Methodology, Formal analysis. **Alessandro Baraldi:** Writing – review & editing, Writing – original draft, Supervision, Project administration, Methodology, Investigation, Funding acquisition, Conceptualization.

Declaration of competing interest

The authors declare that they have no known competing financial interests or personal relationships that could have appeared to influence the work reported in this paper.

Data availability

Data will be made available on request.

Acknowledgments

L.B., D.A. and A.B. acknowledge funding from the MUR PRIN Project 20222FXZ33, “Materials modelling for energy storage applications”, financed by the European Union through the Next generation EU initiative. A.B. acknowledges the financial support from the Quantum Science and Technology Institute, Italy (PNRR MUR Project PE0000023-NQSTI).

Appendix A. Supplementary data

Supplementary material related to this article can be found online at https://doi.org/10.1016/j.surfin.2024.104791.

References

[1] W.-L. Li, X. Chen, T. Jian, T.-T. Chen, J. Li, L.-S. Wang, From planar boron clusters to borophenes and metalloborophenes, Nat. Rev. Chem. 1 (2017) 0071.
[2] A.J. Mannix, Z. Zhang, N.P. Guisinger, B.I. Yakobson, M.C. Hersam, Borophene as a prototype for synthetic 2D materials development, Nat. Nanotechnol. 13 (2018) 444–450.
[3] P. Ranjan, J.M. Lee, P. Kumar, A. Vinu, Borophene: New sensation in flatland, Adv. Mater. 32 (2020) 2000531.
[4] C. Hou, G. Tai, Z. Wu, J. Hao, Borophene: Current status, challenges and opportunities, ChemPlusChem 85 (2020) 2186–2196.
[5] M. Ou, X. Wang, L. Yu, C. Liu, W. Tao, X. Ji, L. Mei, The emergence and evolution of borophene, Adv. Sci. 8 (2021) 2001801.
[6] Z. Xie, X. Meng, X. Li, W. Liang, W. Huang, K. Chen, J. Chen, C. Xing, M. Qiu, B. Zhang, G. Nie, N. Xie, X. Yan, H. Zhang, Two-dimensional borophene: Properties, fabrication, and promising applications, Research 2020 (2020) 2624617.
[7] Y.V. Kaneti, D.P. Benu, X. Xu, B. Yuliarto, Y. Yamauchi, D. Golberg, Borophene: Two-dimensional boron monolayer: Synthesis, properties, and potential applications, Chem. Rev. 122 (2022) 1000–1051.
[8] H. Tang, S. Ismail-Beigi, Novel precursors for boron nanotubes: The competition of two-center and three-center bonding in boron sheets, Phys. Rev. Lett. 99 (2007) 115501.
[9] E.S. Penev, S. Bhowmick, A. Sadrzadeh, B.I. Yakobson, Polymorphism of two-dimensional boron, Nano Lett. 12 (2012) 2441–2445.
[10] Z.A. Piazza, H.-S. Hu, W.-L. Li, Y.-F. Zhao, J. Li, L.-S. Wang, Planar hexagonal B_{36} as a potential basis for extended single-atom layer boron sheets, Nature Commun. 5 (2014) 3113.

[11] B. Albert, H. Hillebrecht, Boron: Elementary challenge for experimenters and theoreticians, Angew. Chem. - Int. Ed. 48 (2009) 8640–8668.
[12] X. Wu, J. Dai, Y. Zhao, Z. Zhuo, J. Yang, X.C. Zeng, Two-dimensional boron monolayer sheets, ACS Nano 6 (2012) 7443–7453.
[13] X.-F. Zhou, X. Dong, A.R. Oganov, Q. Zhu, Y. Tian, H.-T. Wang, Semimetallic two-dimensional boron allotrope with massless dirac fermions, Phys. Rev. Lett. 112 (2014) 085502.
[14] M. Nakhaee, S.A. Ketabi, F.M. Peeters, Tight-binding model for borophene and borophane, Phys. Rev. B 97 (2018) 125424.
[15] B. Feng, O. Sugino, R.-Y. Liu, J. Zhang, R. Yukawa, M. Kawamura, T. Iimori, H. Kim, Y. Hasegawa, H. Li, L. Chen, K. Wu, H. Kumigashira, F. Komori, T.-C. Chiang, S. Meng, I. Matsuda, Dirac fermions in borophene, Phys. Rev. Lett. 118 (2017) 096401.
[16] Y. Zhao, S. Zeng, J. Ni, Phonon-mediated superconductivity in borophenes, Appl. Phys. Lett. 108 (2016) 242601.
[17] M. Gao, Q.-Z. Li, X.-W. Yan, J. Wang, Prediction of phonon-mediated superconductivity in borophene, Phys. Rev. B 95 (2017) 024505.
[18] V. Wang, W.T. Geng, Lattice defects and the mechanical anisotropy of borophene, J. Phys. Chem. C 121 (2017) 10224–10232.
[19] M. Gao, X.-W. Yan, J. Wang, Z.-Y. Lu, T. Xiang, Electron–phonon coupling in a honeycomb borophene grown on Al(111) surface, Phys. Rev. B 100 (2019) 024503.
[20] A.J. Mannix, X.F. Zhou, B. Kiraly, J.D. Wood, D. Alducin, B.D. Myers, X. Liu, B.L. Fisher, U. Santiago, J.R. Guest, M.J. Yacaman, A. Ponce, A.R. Oganov, M.C. Hersam, N.P. Guisinger, Synthesis of borophenes: Anisotropic, two-dimensional boron polymorphs, Science 350 (2015) 1513–1516.
[21] B. Feng, J. Zhang, Q. Zhong, W. Li, S. Li, H. Li, P. Cheng, S. Meng, L. Chen, K. Wu, Experimental realization of two-dimensional boron sheets, Nature Chem. 8 (2016) 563–568.
[22] W. Li, K. Wu, L. Chen, Epitaxial growth of borophene on substrates, Prog. Surf. Sci. (2023) 100704.
[23] A.V. Krasheninnikov, When defects are not defects, Nature Mater. 17 (2018) 757–758.
[24] X. Sun, X. Liu, J. Yin, J. Yu, Y. Li, Y. Hang, X. Zhou, M. Yu, J. Li, G. Tai, W. Guo, Two-dimensional boron crystals: Structural stability, tunable properties, fabrications and applications, Nano Res. 27 (2017) 826–833.
[25] Z. Zhang, Y. Yang, G. Gao, B.I. Yakobson, Two-dimensional boron monolayers mediated by metal substrates, Angew. Chem. - Int. Ed. 127 (2015) 13214–13218.
[26] H. Shu, F. Li, P. Liang, X. Chen, Unveiling the atomic structure and electronic properties of atomically thin boron sheets on an Ag(111) surface, Nanoscale 8 (36) (2016) 16284–16291.
[27] S. Xu, Y. Zhao, J. Liao, X. Yang, H. Xu, The nucleation and growth of borophene on the Ag(111) surface, Nano Res. 9 (2016) 2616–2622.
[28] S. Deng, V. Berry, Wrinkled, rippled and crumpled graphene: An overview of formation mechanism, electronic properties, and applications, Mater. Today 19 (4) (2016) 197–212.
[29] A. Baraldi, G. Comelli, S. Lizzit, M. Kiskinova, G. Paolucci, Real-time X-ray photoelectron spectroscopy of surface reactions, Surf. Sci. Rep. 49 (2003) 169–224.
[30] S. Doniach, M. Sunjic, Many-electron singularity in X-ray photoemission and X-ray line spectra from metals, J. Phys. C: Solid State Phys. 3 (1970) 285–291.
[31] J. Végh, The analytical form of the Shirley-type background, J. Electron Spectrosc. Relat. Phenom. 46 (1988) 411–417.
[32] F.J.G.d. Abajo, M.A.V. Hove, C.S. Fadley, Multiple scattering of electrons in solids and molecules: A cluster-model approach, Phys. Rev. B 63 (2001) 075404.
[33] D. Woodruff, Adsorbate structure determination using photoelectron diffraction: Methods and applications, Surf. Sci. Rep. 62 (2007) 1–38.
[34] J.B. Pendry, Reliability factors for LEED calculations, J. Phys. C Solid State Phys. 13 (2000) 937.
[35] G. Kresse, J. Furthmüller, Efficient iterative schemes for ab-initio total-energy calculations using a plane-wave basis set, Phys. Rev. B 54 (16) (1996) 11169, 11186.
[36] P.E. Blöchl, Projector augmented-wave method, Phys. Rev. B 50 (24) (1994) 17953, 17979.
[37] J.P. Perdew, K. Burke, M. Ernzerhof, Generalized gradient approximation made simple, Phys. Rev. Lett. 77 (18) (1996) 3865, 3868.
[38] G.P. Campbell, A.J. Mannix, J.D. Emery, T.-L. Lee, N.P. Guisinger, M.C. Hersam, M.J. Bedzyk, Resolving the chemically discrete structure of synthetic borophene polymorphs, Nano Lett. 18 (2018) 2816, 2821.
[39] Q. Li, V.S.C. Kolluru, M.S. Rahn, E. Schwenker, S. Li, R.G. Hennig, P. Darancet, M.K.Y. Chan, M.C. Hersam, Synthesis of borophane polymorphs through hydrogenation of borophene, Science 371 (2021) 1143–1148.
[40] B. Kiraly, X. Liu, L. Wang, Z. Zhang, A.J. Mannix, B.L. Fisher, B.I. Yakobson, M.C. Hersam, N.P. Guisinger, Borophene synthesis on Au(111), ACS Nano 13 (2019) 3816–3822.
[41] N.A. Vinogradov, A. Lyalin, T. Taketsugu, A.S. Vinogradov, A. Preobrajenski, Single-phase borophene on Ir(111): Formation, structure, and decoupling from the support, ACS Nano 13 (12) (2019) 14511–14518.
[42] C. Busse, P. Lazić, R. Djemour, J. Coraux, T. Gerber, N. Atodiresei, V. Caciuc, R. Brako, A.T. N'Diaye, S. Blügel, J. Zegenhagen, T. Michely, Graphene on Ir(111): Physisorption with chemical modulation, Phys. Rev. Lett. 107 (2011) 036101.
[43] T. Susi, M. Kaukonen, P. Havu, M.P. Ljungberg, P. Ayala, E.I. Kauppinen, Core level binding energies of functionalized and defective graphene, Beilstein J. Nanotechnol. 5 (2014) 121–132.
[44] D.P. Woodruff, Surface structural information from photoelectron diffraction, J. Electron Spectrosc. Relat. Phenom. 178–179 (2010) 186, 194.
[45] S. Lizzit, G. Zampieri, L. Petaccia, R. Larciprete, P. Lacovig, E.D.L. Rienks, G. Bihlmayer, A. Baraldi, P. Hofmann, Band dispersion in the deep 1s core level of graphene, Nat. Phys. 6 (2010) 345–349.
[46] H. Bana, E. Travaglia, L. Bignardi, P. Lacovig, C.E. Sanders, M. Dendzik, M. Michiardi, M. Bianchi, D. Lizzit, F. Presel, D.D. Angelis, N. Apostol, P.K. Das, J. Fujii, I. Vobornik, R. Larciprete, A. Baraldi, P. Hofmann, S. Lizzit, Epitaxial growth of single-orientation high-quality MoS_2 monolayers, 2D Mater. 5 (2018) 035012.
[47] L. Bignardi, S.K. Mahatha, D. Lizzit, H. Bana, E. Travaglia, P. Lacovig, C. Sanders, A. Baraldi, P. Hofmann, S. Lizzit, Anisotropic strain in epitaxial single-layer molybdenum disulfide on Ag(110), Nanoscale 13 (2021) 18789–18798.
[48] L. Bignardi, D. Lizzit, H. Bana, E. Travaglia, P. Lacovig, C.E. Sanders, M. Dendzik, M. Michiardi, M. Bianchi, M. Ewert, L. Bußß, J. Falta, J.I. Flege, A. Baraldi, R. Larciprete, P. Hofmann, S. Lizzit, Growth and structure of singly oriented single-layer tungsten disulfide on Au(111), Phys. Rev. Mater. 3 (2019) 014003.
[49] L. Bignardi, P. Lacovig, R. Larciprete, D. Alfè, S. Lizzit, A. Baraldi, Exploring 2D materials at surfaces through synchrotron-based core-level photoelectron spectroscopy, Surf. Sci. Rep. 78 (2023) 100586.
[50] M.V. Kuznetsov, I.I. Ogorodnikov, D.Y. Usachov, C. Laubschat, D.V. Vyalikh, F. Matsui, L.V. Yashina, Photoelectron diffraction and holography studies of 2D materials and interfaces, J. Phys. Soc. Japan 87 (2018) 061005.
[51] F. Orlando, P. Lacovig, L. Omiciuolo, N.G. Apostol, R. Larciprete, A. Baraldi, S. Lizzit, Epitaxial growth of a single-domain hexagonal boron nitride monolayer, ACS Nano 8 (2014) 12063–12070.
[52] P. Sang, Q. Wang, W. Wei, Y. Li, J. Chen, Hydrogenated borophene as a promising two-dimensional semiconductor for nanoscale field-effect transistors: A computational study, ACS Appl. Nano Mater. 4 (2021) 11931–11937.
[53] Y. Xu, X. Xuan, T. Yang, Z. Zhang, S.-D. Li, W. Guo, Quasi-freestanding bilayer borophene on Ag(111), Nano Lett. 22 (2022) 3488–3494.
[54] L. Li, J.F. Schultz, S. Mahapatra, X. Liu, X. Zhang, M.C. Hersam, N. Jiang, Atomic-scale insights into the interlayer characteristics and oxygen reactivity of bilayer borophene, Angew. Chem. - Int. Ed. 135 (2023).
[55] X. Liu, M.S. Rahn, Q. Ruan, B.I. Yakobson, M.C. Hersam, Probing borophene oxidation at the atomic scale, Nanotechnology 33 (2022) 235702.
[56] Y. He, N. Cheng, C. Chen, S. Xiong, J. Zhao, Tuning the electronic transport anisotropy in borophene via oxidation strategy, Sci. China Technol. Sci. 62 (5) (2019) 799–810.
[57] L. Shi, C. Ling, Y. Ouyang, J. Wang, High intrinsic catalytic activity of two-dimensional boron monolayers for the hydrogen evolution reaction, Nanoscale 9 (2) (2016) 533–537.
[58] C. Liu, Z. Dai, J. Zhang, Y. Jin, D. Li, C. Sun, Two-dimensional boron sheets as metal-free catalysts for hydrogen evolution reaction, J. Phys. Chem. C 122 (33) (2018) 19051–19055.